IX Lifetimes of Excited States in Highly Charged Ions

Lorenzo J. Curtis and Indrek Martinson

Summary. The experimental measurement and theoretical formulation of atomic lifetimes are being extended to systems that have both many electrons stripped away and multiple electrons remaining. The dynamical structure of these systems can be significantly affected by interactions that are negligible in neutral and few-times ionized systems, and the lifetimes can sensitively probe interelectron correlations, relativistic and quantum electrodynamic interactions, and effects of the finite size of the nucleus. These interactions often have characteristic dependencies on the central charge, and studies of systematic trends can reveal both predictive regularities and theoretical insights. Besides providing new tests of atomic theory, these systems have important applications in astrophysics, in fusion plasma technology, and in XUV-laser development.

1. Introduction

The availability of fundamental atomic lifetime data has a significant impact on progress in other fields of science and in areas of modern technology, e.g., in fundamental physics and precise measurements, in the generation of coherent light, in solar physics and astrophysics, and in plasma diagnostics. The accurate specification of energy levels and transition probabilities for ionized atoms has important immediate applications. One application concerns the diagnosis and modeling of controlled fusion plasmas, both in the central region and in the region of the edge plasma. Transition probabilities are necessary both to determine concentrations of impurity elements and to predict the rates of dielectronic recombination, radiative cooling, etc. [1]. They are also needed in the development of XUV lasers and in the interpretation of atomic collision studies. These data are also essential to the determination of elemental abundances in the interpretation of the spectra of astrophysical objects. These objects are important both as working examples of energy production, and as light sources for spectroscopic investigations. This area has expanded rapidly since the deployment of the Goddard High Resolution Spectrograph on board the Hubble Space Telescope [2], and other facilities such as SUMER (the Solar Ultraviolet Measurement of Emitted Radiation) on SOHO (the Solar and Heliospheric Observatory) [3]. These instruments have yielded many interesting and sometimes unexpected results which require additional atomic data for their interpretation.

Progress in the spectroscopy and time resolved structure of multiply ionized atoms has been greatly enhanced by the development of new light sources and technical advances in the use of traditional light sources, motivated by urgent needs in specific applications. These light sources involve the use of

fast ion beams, tokamak- and laser-produced plasmas, orbiting observation of astrophysical objects, recoil ions from ion–atom collisions, electron beam ion sources (EBIS) and ion traps (EBIT), electron cyclotron resonance (ECR) ion sources, ion storage rings and Fourier transform spectroscopy (FTS), as well as improved use of traditional spark, vacuum arc, and laser-produced plasma sources. Since the interpretation of time resolved measurements often requires a thorough understanding of the radiatively coupled energy level structure, they must proceed in concert with high resolution wavelength and energy level measurements.

Highly ionized atomic systems involve new theoretical regimes, where interactions that are negligible in neutral atoms can become dominant. Because they scale with different powers of the nuclear charge Z, relativistic and quantum electrodynamic (QED) interactions can become very large in these systems. Traditionally "forbidden" decay processes such as M1, E2, M2, and two photon decay (2E1) can exceed "allowed" E1 processes because of their stronger Z scaling. Rather than being exotic, these highly ionized systems dominate high temperature environments such as the solar corona and stellar and laboratory plasmas, and thus almost all matter in the universe is in the ionized state. In such systems the electron binding energy is very large, and the strong Coulomb field has a long-range intensity that enhances interaction cross sections. The reduced electron screening causes inner shell effects to become more important. All of these properties are dependent on Z, which can be treated as a controllable experimental parameter if a sufficiently large and reliable data base can be followed along an isoelectronic sequence.

To prescribe these systems, calculational methods must sometimes undergo conceptual and computational refinements subject to experimental verification. Furthermore, the accurate specification of wavelength and energy level data does not insure correct predictions of transition probabilities and lifetimes. Measurements of the lifetimes are particularly important, since they provide absolute rate values necessary to normalize relative transition probabilities obtained by time-integrated techniques.

A key feature of the specification of transition probability rates in highly ionized atoms is the use of semiempirical parametrization as a predictive tool. The search for systematic behavior in existing data and the use of previously discovered systematics in the interpretation of new data has long been a primary methodology of atomic spectroscopy. These tendencies have been accelerated by the size and precision of the available data base. It is now possible to select subsets within large blocks of atomic data so as to probe a specific property, e.g. along an isoelectronic, isonuclear, homologous, or Rydberg sequence, or along an yrast chain. This can reveal unexpected regularities (or unexpected departures from known regularities) that would otherwise go unnoticed. This sensitivity can be enhanced using data-based semiempirical systematizations, which amplify subtle interactions by reex-

pressing them as an effective parameter in a simple independent particle mapping reduction.

This review will attempt to describe the current status of this field and to provide a few illustrative examples of recent results. For more details, the reader is referred to a number of recent reviews [4–13].

2. Experimental Methods

2.1 Excitation Methods

The most direct method for the experimental determination of level lifetimes is through the time resolved measurement of the free decay of the fluorescence radiation following a cutoff of the source of excitation. An important factor limiting the accuracy is the repopulation of the level of interest by cascade transitions from higher lying levels, which can produce multiexponential decay curves that are difficult to analyze with precision by standard curve fitting methods. To circumvent this limitation, two alternative methods are often employed. One involves selective excitation of the level of interest, thus eliminating cascading altogether; another uses correlations between cascade connected decays to account in detail for the effects of cascades.

While selective excitation methods totally eliminate the effects of cascade repopulation, they are generally limited to levels in neutral and singly ionized atoms that can be accessed from the ground state by strongly absorptive E1 transitions, and the selectivity itself is a limitation. Many very precise measurements have been made [5] by these techniques, frequently for Δn=0 resonance transitions in neutral alkali atoms and singly ionized alkali-like ions.

More general access can be obtained by nonselective excitation methods, such as pulsed electron beam bombardment of a gas cell or gas jet, or in-flight excitation of a fast ion beam by a thin foil. Pulsed electron excitation methods are well suited to measurements in neutral and near neutral ions (although for very long lifetimes in ionized species, the decay curves can be distorted if particles escape from the viewing volume through thermal migration or the Coulomb explosion effect [14]). Nonselective excitation techniques can also be applied to measurements such as the phase shift method and the Hanle effect, in which case cascade repopulation can also be a serious problem [15]. In the case of highly ionized atoms, the only generally applicable method of lifetime determination is by beam foil spectroscopy (BFS), the thin foil excitation of a fast ion beam. However, additional techniques, e.g., using recoil ions [16], ion traps and storage rings, have been employed in recent years for the determination of long lifetimes (cf. Sect. 6).

In beam-foil studies, excitation of the ions occurs in the dense environment of the foil, after which they emerge into a field free, collision free, high vacuum region. A time-resolved decay curve is obtained by translating the foil

relative to the detection apparatus. The beam is a very tenuous plasma, which has both advantages and disadvantages. The low density avoids the effects of collisional de-excitation and radiation trapping, but produces relatively low light levels. This requires fast optical systems with reduced wavelength resolution, which can lead to blending of the Doppler broadened lines. Methods have been developed to refocus the monochromator to a moving light source, using the angular dependence of the Doppler shift to narrow and enhance the lines. Detailed descriptions of the various aspects of beam foil lifetime measurements can be found in Refs. [6, 8, 17].

2.2 Data Analysis

Due to the nonselective nature of beam-foil excitation, the level populations (and hence the decay curves) are affected by cascade repopulation. Thus, the decay curve involves a sum of many exponentials, one corresponding to the primary level, and one to each level that cascades (either directly or indirectly) into it. Decay exponentials do not comprise an orthogonal set of functions, and the representation of an infinite sum by a finite sum through curve fitting methods [18] can, in unfavorable cases, lead to significant errors, sometimes as large as 30–40%. Thus, while cascades which differ significantly in lifetime from that of the primary do not pose a serious problem, when the cascades and primary have similar lifetimes their contributions can seriously distort the decay curve.

Fortunately, alternative methods to exponential curve fitting exist, which permit the accurate extraction of lifetimes to be made from correlated sets of nonselectively populated decay curves. Situations in which cascading is dominated by a few strong decay channels are ideally suited to the arbitrarily normalized decay curve (ANDC) method [19, 17]. This method exploits dynamical correlations among the cascade-related decay curves, which arise from the rate equation that connects the population of a given level to those of the levels that cascade directly into it. The instantaneous population of each level is, to within constant factors involving the transition probabilities and detection efficiencies, proportional to the intensity of radiation emitted in any convenient decay branch. A joint correlated analysis of the decay curves of the primary level and those of the levels that directly repopulate it yields both the primary lifetime and the intensity normalizations of the cascades relative to that of the primary.

A schematic representation of the ANDC method, applied [20] to the resonance transition of Tl III in the Au isoelectronic sequence, is shown in Fig. 1. The study of lifetimes in ions of very heavy elements such as Tl has been motivated by their occurrence in the spectra of certain chemically peculiar stars [2]. The inset decay curves indicate that the arbitrarily normalized decay curves $I_{6p}(t)$ of the $6p\ ^2P_{3/2}$ level and its cascades from the $6d\ ^2D_{5/2}$ and $7s\ ^2S_{1/2}$ are jointly analyzed using the population equation expressed in the form

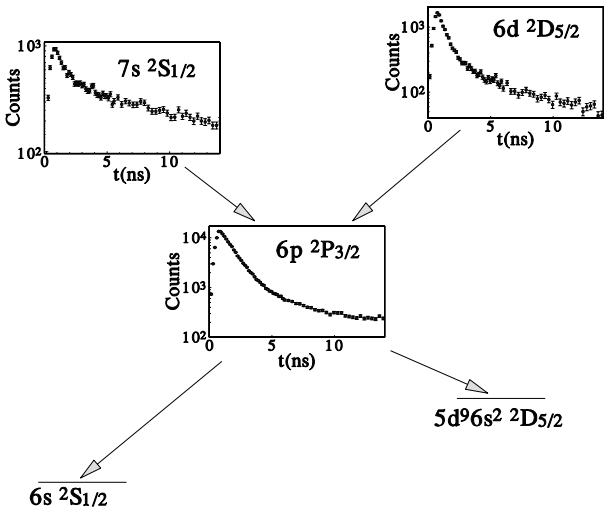

Fig. 1. Schematic plot of the ANDC analysis of the $6s$–$6p$ transition in Tl III

$$\tau_{6p}\frac{dI_{6p}}{dt}(t_i) = \xi_{6d}I_{6d}(t_i) + \xi_{7s}I_{7s}(t_i) - I_{6p}(t_i)\ . \tag{1}$$

Here the primary lifetime τ_{6p} and the relative normalizations ξ_{6d} and ξ_{7s} for the cascade and primary decay curves are determined by simultaneous solution of the large set of relationships provided by (1) evaluated at each of the common points t_i on the decay curves. If all significant direct cascades have been included, the goodness-of-fit will be uniform for all time subregions, indicating reliability. If important cascades have been omitted or blends are present, the fit will vary over time subregions, indicating a failure of the analysis. Very rugged algorithms have been developed [21] that permit accurate lifetimes to be extracted even in cases where statistical fluctuations are substantial. The use of the ANDC method can provide a striking improvement in the reliability of the lifetime extracted from the decay curves. In a recent study of the lifetime of the $3s3p\ ^1P_1$ level in Mg-like Cl VI, *Engström* et al. [22] obtained a value 0.24±0.02 ns from curve fitting and a value of 0.165±0.009 ns from ANDC, a nearly 50% over-estimation by curve fitting.

2.3 Detection Methods

The use of position sensitive detection (PSD) to make simultaneous measurements of many different decay curves is an advance that has made possible many new types of experiments in fast ion beam spectroscopy. These multiplexed methods greatly enhance the data collection efficiency for this low density light source, and cause many possible systematic errors to cancel in differential measurements. Examples of new types of measurements that can be made using this technology include studies of: (a) the variation of lifetimes among fine structure components within a multiplet that occur due to, e.g.,

selective access to forbidden intercombination and autoionization channels; and (b) analysis of decay curves in a cascade chain using the ANDC method [19, 17]. If the intensities of a group of lines that are, e.g., within a multiplet, connected by a cascade scheme, overlapping in a blend, etc. are recorded simultaneously, effects such as fluctuations in the beam current, degradation of the foil, divergence of the beam, etc., will affect all of the decay curves in the same way, and vanish from the differential decay curves.

In these measurements the PSD is mounted at the exit focus of the analyzing monochromator. Since it records all lines within a wavelength interval simultaneously, it can greatly reduce the required accelerator time. The multichannel detection also provides the advantage of simultaneously measured reference lines (beam foil spectra exhibit sizable Doppler shifts, precluding the use of stationary calibration sources). Decay curves can be constructed by integrating over a line profile, and that profile can be examined for exponential content to eliminate blending. The time dependent backgrounds underlying the decay curves are directly available from the neighboring channels.

One application of this technique [23] concerned the precise measurement of the ratio of lifetimes of the $J = 3/2$ and $1/2$ resonance transitions in Li-like Si. This type of multiplexed decay curve measurement yielded an accuracy in the difference between the two lifetimes that was better than could be obtained for either lifetime separately. Another application [24] studied intercombination transitions (i.e., E1 transitions which violate the $\Delta S = 0$ selection rule) in Mg- and Al-like ions of Br. The time resolved wavelength spectrum provided a common exposition of decays with a wide range of lifetimes. The short-lived decays arising from transitions provided wavelength calibrations, and the long-lived lines arising from intercombination transitions could be used for wavelength and lifetime determinations.

3. Computational Methods

3.1 Definitions

The theoretical quantity that characterizes the spontaneous emission and absorption of radiation between levels i and k is the *line strength* S_{ik}, given in the electric dipole (E1) approximation by the expression [25]

$$S_{ik} = \sum_{m_i} \sum_{m_k} |\langle i|\boldsymbol{r}|k\rangle|^2 , \tag{2}$$

where m_i and m_k are magnetic quantum numbers.

Under the approximations and assumptions of the Weisskopf–Wigner formulation [26], the line strength can be related to the measured exponential lifetime τ_i, provided that the branching fraction B_{ik} for decay from the upper level i to a specific lower level k is known from other measurements. In such a

case an experimental value for S_{ik} can be extracted from the measured data using the relationship

$$S_{ik} = [\lambda_{ik}(\text{Å})/1265.38]^3 g_i B_{ik}/\tau_i(\text{ns}), \tag{3}$$

where λ_{ik} is the transition wavelength and g_i is the upper level degeneracy. In terms of these quantities, the emission of radiation can be specified by the spontaneous transition probability rate A_{ik}

$$A_{ik} = B_{ik}/\tau_i \tag{4}$$

and the absorption of radiation can be specified by the absorption oscillator strength f_{ki}

$$g_k f_{ki} = [303.75/\lambda_{ik}(\text{Å})] S_{ik}, \tag{5}$$

where g_k is the lower level degeneracy.

3.2 Methodologies

In theoretical calculations of transition probabilities and lifetimes for highly charged ions, a number of effects must be considered. In addition to the electron correlation, which also plays an important role in neutral and a few times ionized ions, the effects of relativity, QED and sometimes even nuclear structure have to be incorporated in the calculations. The importance of these additional effects increases strongly with Z which means, for instance, that simplifications based on perturbative treatments may not be adequate in highly charged ions [27].

The theoretical techniques can be roughly divided into two categories, ab-initio calculations and semiempirical methods. In the latter category the wave functions are usually optimized by utilizing accurate experimentally determined data, e.g., excitation energies. This is done in the superposition of configuration (SOC) calculations with the *Cowan* code [25] by a suitable scaling of the Slater parameters. This method has been successfully applied to ions with complex electron structure where ab-initio calculations may encounter substantial computational difficulties. Another semiempirical technique, the Coulomb approximation with Hartree–Slater core (CAHS) method which incorporates a realistic model potential to account for polarizability, spin–orbit interaction and exchange effects [28] has yielded quite accurate f-value data, in particular for ions with a few active electrons. Extensive sets of data for multiply ionized atoms have also been obtained by means of the so-called MZ method, a Z-expansion technique based on perturbation theory [29], the results being quite accurate even for very high charge states.

Among the various ab-initio methods, those based on the multiconfiguration Hartree–Fock (MCHF) [30] or configuration interaction (CI) [31] treatments have in recent years provided very accurate data, e.g., for Be-like ions, where f-values with uncertainties as low as 2–3% have been predicted [32, 33]. The theoretical methods mentioned so far are basically nonrelativistic, but

relativistic effects can usually be incorporated within the Breit–Pauli approximation [34], whereby the relativistic part of the Hamiltonian is added to the nonrelativistic one. However, fully relativistic calculations are now often performed for highly charged ions. The multiconfiguration Dirac-Fock (MCDF) method [35] is thereby frequently used. Another powerful program is the multiconfiguration relativistic random-phase approximation (MCRRPA), introduced in the early 1980s [36]. Recent results of calculations with this method concern Be-like ions [37]. Also, the many-body perturbation theory (MBPT), applied to atomic physics problems in the early 1960s, has in recent years been successfully extended to the relativistic regime [38, 39]. However, while the fully relativistic programs are very efficient when applied to highly charged ions, they are less powerful for lower ionization stages because they can usually treat electron correlation effects in a comparatively limited way.

4. Semiempirical Systematizations

Much progress in the evaluation, interpolation and extrapolation of atomic transition probability rate data has been achieved through systematic studies along isoelectronic sequences. For example, it has been observed [40] that for low to intermediate values of Z, a smooth isoelectronic variation is often obtained when the quantity f_{ik} is plotted for an isoelectronic sequence versus the quantity $1/Z$. However, as experimental measurements have been extended to very high stages of ionization, it has been found that a more extensive and more nearly linear exposition results when experimental values for line strengths are plotted versus an appropriately defined reciprocal effective screened charge. Thus large blocks of isoelectronic data can be described by the equation

$$Z^2 S \cong S_0 + b/(Z - C), \tag{6}$$

where S_0, b and C are empirical constants. In this manner a relatively small number of precision lifetime measurements can be used to interpolatively predict line strengths for entire isoelectronic sequences. A few of the types of sequences which have been systematized by these methods will be described below.

4.1 Alkali-Metal-Like Sequences

Isoelectronic regularities in line strength data for complex atoms were predicted theoretically [41, 42] and were first empirically applied [43] in the study of scaled line strengths for $\Delta n = 0$ resonance transitions in alkali-metal-like systems. For these systems, it has been found that the isoelectronic variation cannot only be linearized, but that the semiempirical fitting parameter S_0 effectively matches the corresponding hydrogenic $\Delta n = 0$ value S_{H}, which is given for an s–p transition by [34]

$$S_0 \to S_{\rm H} = 3n^2(n^2-1)g_i/4. \tag{7}$$

Expositions of the existing data bases for the Li, Na, Cu, and Ag sequences [44] are shown in Fig. 2. (Here, as well as in Figs. 3–6, all experimental data, except for some neutral and singly charged species, originate from beam-foil measurements.) The linearity is achieved by setting the screening parameters at $C = 2.17, 10.0, 25.9, 44.7$ for $n = 2, 3, 4, 5$, respectively. In these systems the ns–np resonance transitions are unbranched, so $B_{ik} = 1$ and the line strengths are determined directly from the measured lifetimes. If the linearity of (6) is valid, then accurate measurements for the lifetimes of a few members of the sequence at low stages of ionization can be interpolated to the hydrogenic limit at high Z, providing accurate estimates for all intervening ions.

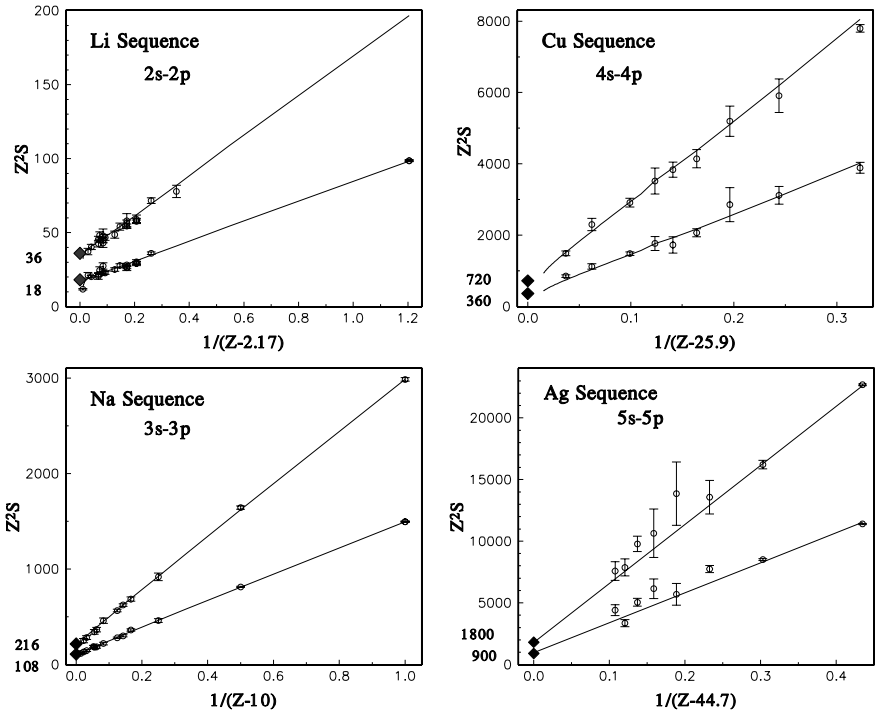

Fig. 2. Scaled line strength plots for the ns–np transitions in the alkali-like Li, Na, Cu and Ag sequences. Data sources are given in Ref. [44]

While these expositions exhibit empirical linearities for low to medium degrees of ionization, the hydrogen-like value given in (7) is nonrelativistically computed, and at very high Z this Schrödinger formulation would be expected to break down. Correspondingly, the solution to the Dirac equation for a pure $1/r$ potential is given by

$$Z^2 S = S_{\mathrm{H}}[1 - \sum_i a_i (\alpha Z)^{2i}], \tag{8}$$

where S_{H} is as given by (7) and a_i is a set of coefficients given in Ref. [44]. An experimental test of this high Z behavior is available for the Li sequence, where the $2p^2 P_{1/2}$ lifetime has been measured for lithium-like uranium U^{89+} [45]. As can be seen from the lithium-like case in Fig. 2 and the blowup of its high-Z region in Fig. 3a, the three-electron uranium measurement falls considerably below the linear trend. This discrepancy disappears, however, when the semiempirical exposition is modified to take into account the high-Z behavior of the corresponding hydrogen-like system, using the form

$$Z^2 S / [1 - \sum_i a_i (\alpha \{Z - C\})^{2i}] \cong S_{\mathrm{H}} + b/(Z - C). \tag{9}$$

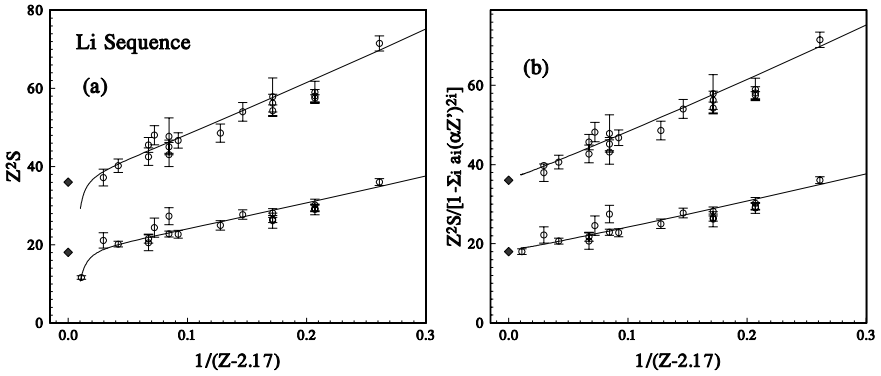

Fig. 3. Scaled line strengths for the Li $2s$–$2p$ sequence, without (a) and with (b) relativistic hydrogenic corrections. Data sources are given in Ref. [44]

As can be seen from Fig. 3b, this modification restores linearity to the exposition, and allows the existing data base to be used to accurately specify line strengths for the entire isoeletronic sequence.

4.2 Alkaline-Earth-Like Sequences

In the case of systems in which two valence electrons (or one electron and one hole) occur in an otherwise closed shell core, a simple extension of this formalism has been developed that combines lifetime data for the resonance and intercombination lines. In systems such as ns^2–$nsn'p$ and np^6–$np^5 n's$, both the $^1S_0$–$^1P_1$ and $^1S_0$–$^3P_1$ transitions occur because intermediate coupling (IC) causes spin hybridization of the nominally singlet and triplet excited states. In the absence of strong configuration interaction (CI) effects, the IC amplitudes can be determined from spectroscopic energy level data and expressed

in the form of a singlet-triplet mixing angle θ. The measured lifetime data for the unbranched resonance and intercombination lines are first converted to line strengths $S(Res)$ and $S(Int)$ using (3), and then reduced to the effective values

$$S_{\rm r}({\rm Res}) \equiv S({\rm Res})/\cos^2\theta, \tag{10}$$

$$S_{\rm r}({\rm Int}) \equiv S({\rm Int})/\sin^2\theta, \tag{11}$$

from which the effects of IC have been removed. Empirical plots of data that have been reduced in this way are shown in Fig. 4 for the ns^2–$nsnp$ transitions in the Mg [46], Zn [47], Cd [48], and Hg [49] sequences. Linear plots are achieved by use of the screening parameters $C = 10.5$, 28, 46, 75 for $n = 3, 4, 5, 6$. Here both $J = 1$ levels tend to converge to a value of $S_{\rm H}$ twice that predicted by (7) (consistent with the two equivalent ground term electrons).

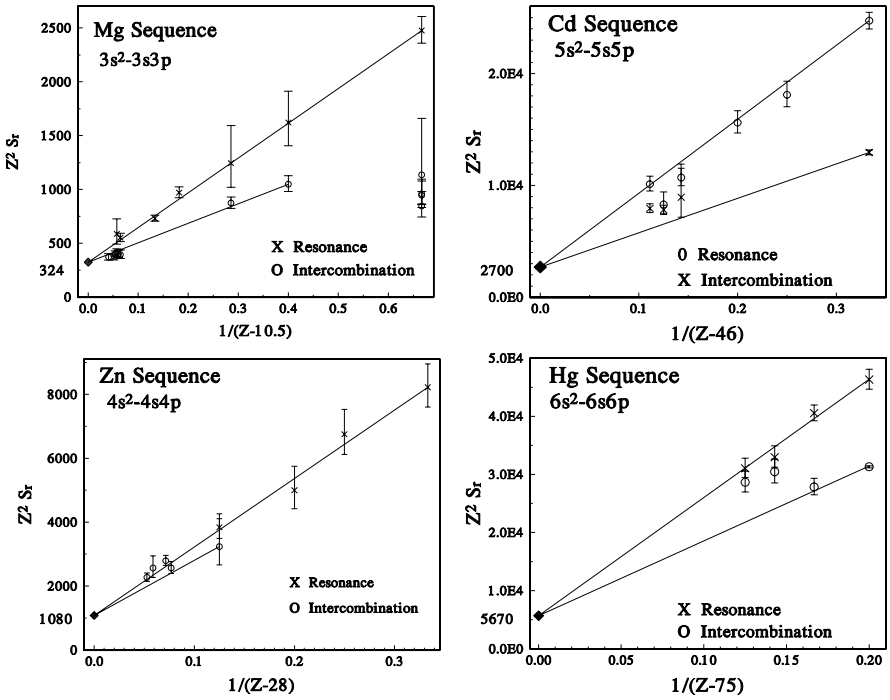

Fig. 4. Screened line strength exposition for the ns^2–$nsnp$ transitions in the Mg, Zn, Cd and Hg sequences. Data sources are given in Refs. [46-49]

In these two valence electron cases, the question arises as to whether the data should be extrapolated to high Z using the single-configuration hydrogenic value, or take into account the CI that can occur due to the

hydrogenic degeneracy of levels within the same complex. *Curtis* and *Ellis* [50] have studied this for the Be sequence, which they have characterized by two mixing angles: ϕ (the high Z asymptotic limit of the CI mixing between $2s^2$ and $2p^2$) and θ (the IC mixing between the singlet and triplet J=1 levels in $2s2p$). They achieved a linear systematization of the data by theoretically calculating the nonrelativistic high Z limit of the $2s^2$–$2p^2$ mixing angle, which yielded ϕ=13° [50]. This predicts a high Z result $S_{\rm H}$ = 38.5, which agrees very well with the trend of the measured data shown in Fig. 5a.

Studies have also been made [51] within this semiempirical formulation to characterize the differences between the radial dipole matrix elements for the resonance and intercombination transitions. *Curtis* et al. [51] have shown that for a Dirac relativistic formulation of the ns^2–$nsn'p$ transition, the line strengths can be specified in terms of the J = 1/2–3/2 and J=1/2 –1/2 radial matrix elements R_{31}=$\langle s_{1/2}|r|p_{3/2}\rangle$ and R_{11}=$\langle s_{1/2}|r|p_{1/2}\rangle$ by

$$S_{\rm r}({\rm Res}) \equiv S({\rm Res})/\cos^2(\theta-\xi), \tag{12}$$

$$S_{\rm r}({\rm Int}) \equiv S({\rm Int})/\sin^2(\theta-\xi), \tag{13}$$

where

$$\tan\xi \equiv \sqrt{2}(R_{31}-R_{11})/(2R_{31}+R_{11}). \tag{14}$$

Figure 5b shows the data for the $2s^2$–$2s2p$ transitions in the Be sequence with these additional relativistic corrections, which remove the gap between resonance and intercombination transition data. Thus, with these corrections, the combined data base for the resonance and intercombination lines can be used to predict the lifetimes of both the singlet and triplet J = 1 levels for the entire isoelectronic sequence.

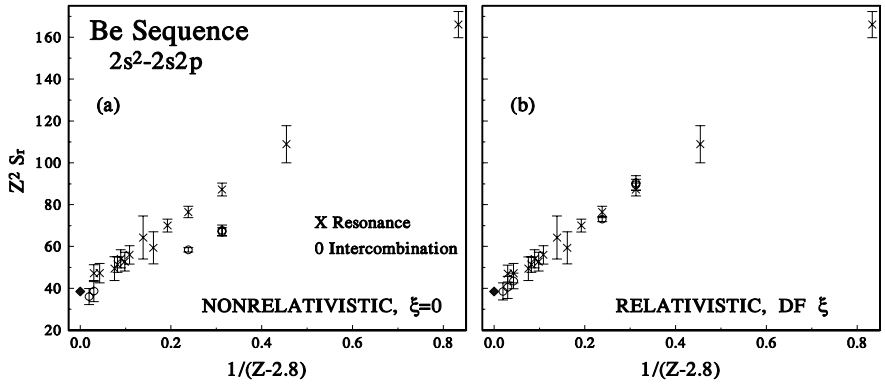

Fig. 5. Scaled line strengths for the Be $2s^2$–$2s2p$ sequence with corrections for (a) asymptotic CI between $2s^2$ and $2p^2$ and (b) with relativistic corrections for the J-dependence of the Dirac wave functions. Data sources are given in Ref. [50]

4.3 Intershell $\Delta n = 1$ Line Strengths

All of the cases discussed above involve intrashell $\Delta n = 0$ transitions (ns–np for alkali-metal-like sequences, ns^2–$nsnp$ for alkaline-earth-like sequences) and the next logical step would be to extend the formalism to $\Delta n > 0$ transitions. Unfortunately, this is not generally possible because almost no measured transition probability data exist for $\Delta n > 0$ transitions in multiply charged ions. This results from the fact that decay rate data for multiply charged ions consist almost exclusively of lifetime measurements. These can be used to deduce transition probabilities for unbranched decays, but (as discussed in Sect. 5) virtually no branching fraction measurements exist for multiply charged ions. Two counterexamples exist, in which special conditions permit the determination of line strengths from lifetimes for $\Delta n = 0$ transitions.

The first example involves the $2s^2\ {}^1S_0$–$2s3p\ {}^{1,3}P_1$ transitions in the Be isoelectronic sequence [52]. Here differential lifetime measurements in the $2s3s\ {}^3S_1$–$2s3p\ {}^3P_{2,1,0}$ decay channels determine the intercombination branch to ground as an extra channel available only to the ${}^3P_1$ level. This decay mode is made possible by the spin–orbit interaction which mixes the ${}^1P_1$ and ${}^3P_1$ levels. For the resonance transition, the ${}^1P_1$ level decays dominantly to the ground state, and other branching can be estimated theoretically without large error. The second example involves the $2p^6\ {}^1S_0$–$2p^5 3s\ {}^{1,3}P_1$ transitions in the Ne sequence [52], for which the first excited state is extrashell, giving rise to unbranched $\Delta n = 1$ resonance and intercombination transitions. Expositions of these data are shown in Fig. 6.

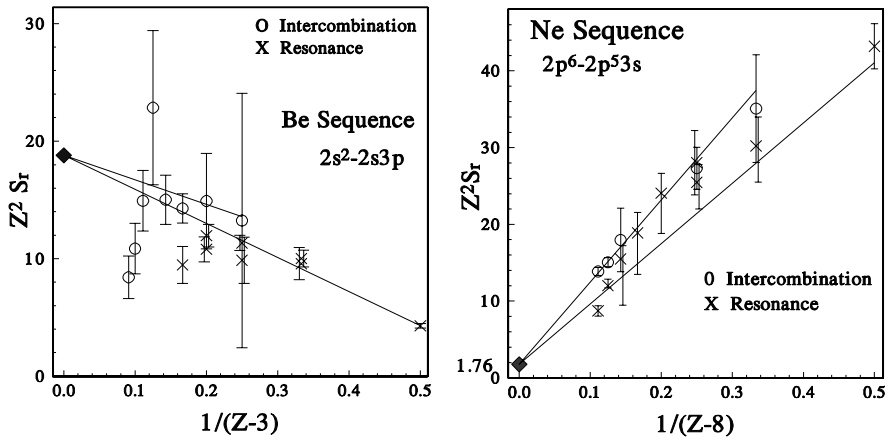

Fig. 6. Scaled line strengths for the $\Delta n = 1$ transitions in the (a) Be $2s^2$–$2s3p$ and (b) Ne $2p^6$–$2p^5 3s$ sequences. Data sources are given in Ref. [52]

Here again the data appear to converge toward the hydrogenic limits at high Z ($S_{\rm H}$ = 18.79 for $2s$–$3p$ and $S_{\rm H}$=1.76 for the $2p$–$3s$). Despite the obvious differences in their structures, striking similarities exist between these two sequences, and they are in some ways more closely related to each other than to other transitions within their own sequence. For example, the isoelectronic behavior of the singlet-triplet mixing angles for these two sequences are virtually identical. Unlike the case for the Be $2s2p$ sequence, both the Be $2s3p$ and the $2p^5 3s$ configurations pass through a value of 45° for the mixing angle, (where the singlet and triplet reverse their roles as the dominant amplitude in the wave function) just above $Z = 20$. These and other interesting properties motivate additional studies of $\Delta n \geq 1$ transitions.

5. Transition Probabilities and Branching Fractions

5.1 The Need for Branching Fractions

Branching fractions are needed to convert lifetime data to transition probabilities and absorption oscillator strengths. These quantities are needed to deduce elemental abundances from astrophysical spectra, to determine impurity concentrations from fusion plasmas spectra, and to make transition-by-transition comparisons between experiment and theory (summed comparisons can conceal the origin of discrepancies).

As discussed above, atomic lifetime measurements can be transformed into a slowly varying isoelectronic systematization by reducing each lifetime to a corresponding effective line strength factor. This is in contrast to the raw measurements, since the reciprocal lifetime of a branched decay consists of a sum of transition probabilities, each with a different wavelength dependence that possesses its own characteristic dependence on Z. Thus, while a branched line strength factor will usually have a simple and slowly varying isoelectronic behavior, a lifetime may have a rapid isoelectronic variation containing several different powers of Z. The line strength reduction requires knowledge of the branching fractions.

Much progress has been made in the determination of branching fractions in neutral and singly ionized atoms, through the use of absolute emission, absorption, or dispersion measurements, or through combined measurements of relative branching ratios and lifetimes [5]. In highly ionized atoms, many measurements of lifetimes in the 1–5% accuracy range have been made by ANDC analysis [19, 17] of beam-foil measurements. However, *branching ratio measurements in multiply charged ions are virtually nonexistent.* This dearth of $\Delta n \geq 1$ ionic transition probability data is not widely recognized, and deserves special emphasis.

5.2 Calibrated Intensity Measurements

The reason for this lack of branching fraction data in multiply charged ions is clear. Most measurement methods require a relative intensity calibration of the detection apparatus as a function of wavelength, and this is particularly difficult for multiply charged ions. Until recently, beam-foil excitation was the only general way of accessing highly ionized systems. With fast ion beam methods there are Doppler broadenings and shifts, polarizations due to anisotropic excitation, wavelengths not amenable to reflective and transmissive optical elements, differential downstream decays and repopulations of the levels, etc. These attributes are not well suited to standard techniques for calibrating grating spectrometers and detection systems through the use of standard lamps. Calibrations have been carried out using synchrotron radiation, or through in-beam lines with known branching fractions, but these techniques are highly specialized and not widely applicable. It is now possible to supplement time-resolved beam-foil studies with measurements of relative intensities from a common upper level using ECR sources, ion traps, and high effect lasers, coupled to both grating and FTS spectrometers, but many similar problems in calibration must also be overcome with these methods. While the calibration of the wavelength dependence of the detection efficiency of an optical system presents many difficulties, these are less severe in the study of neutral and singly charged ions. Here laboratory-fixed calibration sources can be used in some applications, as has been discussed by *O'Brian* and *Lawler* [10].

The use of Si(Li) detectors in the measurement of very short wavelength radiation in highly ionized atoms also offers possibilities for branching ratio measurements. Since these devices can specify the photon energy from pulse height information without the need for a spectrometer, they can be calibrated for detection efficiency as a function of energy. This type of detection was recently used to determine the branching ratio of the M1 channel to the two-photon decay channel in the $2s\ ^2S_{1/2}$ state in the one-electron krypton ion [53].

5.3 Specialized Methods for Determining Branching Fractions

When branching is within a multiplet between two terms that are each dominated by a single configuration, branching fractions can be empirically specified from IC amplitudes deduced from spectroscopic energy level data. Applications of this approach have recently been applied to the Pb sequence [51, 54].

Differential lifetime measurements can also sometimes be used to determine branching fractions. One application involves studies of the lifetimes of the individual fine structure components of a multiplet decay. If one fine structure level has a decay channel that is not available to the other levels (e.g., a spin-changing transition [52] or an autoionization mode [55] made

possible by J-dependent IC) then the transition probability rate of the extra channel can be determined by differential lifetime measurements.

In addition, the correlated analysis of cascade-related decay curves by the ANDC method [17, 19] can yield both the lifetime of the primary level and the detection efficiencies of the cascade decay curves relative to that of the primary. The correlated time structure of the decay curves can therefore provide a relative calibration of the detection equipment as a by-product. This technique has been successfully used [56] to calibrate a detection system at discrete points over the wavelength region λ= 400–5000 Å by bootstrapping successive ANDC analyses in Na-like S VI.

6. Forbidden Transitions

6.1 Experimental Techniques

As indicated in the Introduction, the forbidden transitions (M1, M2, E2, 2E1, spin-forbidden E1, etc.) have very low transition probability rates in neutral or few-times ionized atoms where allowed (E1) transitions dominate. However, the decay rates of the latter scale approximately as Z (for $\Delta n = 0$) and as Z^4 (for $\Delta n = \pm 1$) to be compared with Z^6–Z^{10} for the various forbidden decay modes, which therefore become important in highly charged ions.

In beam-foil experiments the practical lifetime range is approximately 1 ps–200 ns. Measurements of longer lifetimes are cumbersome, partly because the 1/e path lengths become very 1arge. This means that BFS can be used to determine f-values for allowed transitions from neutral atoms up to perhaps 70+ ions (in favorable cases) and for forbidden lines from approximately 15+ and higher charge states. Certain spin-forbidden E1 decays in lower state ions have also been studied by BFS, but such work has also been extended to highly charged systems [57]. However, long lifetimes in multiply charged ions can now be determined by using a number of techniques of more recent origin than BFS. These utilize: ion traps, for instance an EBIT facility, and storage/cooler rings for ions.

At the Livermore EBIT [58] the decay time of an M1 transition from the $1s2s\ ^3S_1$ level in He-like Ne and Mg were determined (cf. Fig. 7b) [59, 60]. This level was excited by a fast-switching electron beam and the fluorescent decay was recorded. The resulting lifetime values, 90.5±1.5 μs (Ne) and 13.61±0.49 μs (Mg), were found to be in good agreement with theoretical predictions. A more complicated system, Ti-like Xe^{32+}, was studied with the EBIT at NIST in Gaithersburg. Here a decay time of an M1 transition between two fine structure levels was determined [61]. The lifetime range that can be determined with EBIT facilities has been estimated to be 10^{-7}–10^{-2} s.

Storage/cooler rings for ions [62–64] are also well suited for the studies of long lifetimes. Using laser-induced fluorescence at the ESR heavy ion cooler

ring at GSI, *Klaft* et al. [65] were able to observe the ground state hyperfine splitting of hydrogen-like $^{209}Bi^{82+}$ and measure the lifetime of the excited component. In studies of lifetimes of the $1s2s\ ^3S_1$ levels in He-like C^{4+} [66] as well as B^{3+} and N^{5+} [67] at the Heidelberg storage ring, fluorescence was not recorded. Instead, the lifetimes were studied by using dielectronic recombination (DR) resonances from collisions between the $1s2s\ ^3S_1$ level and electrons in the electron cooler. Very precise lifetimes, e.g., 20.59±0.05 ms for C^{4+}, were obtained which allowed detailed comparisons between theoretical values. Furthermore, this method has been extended to the Be-like ions C^{2+}, [68], N^{3+} and O^{4+} [69], for which the lifetime of the metastable level $2s2p\ ^3P_1$ has been accurately measured.

6.2 Forbidden Transitions in One- and Two-Electron Ions

Allowed and forbidden transitions between low-lying levels in H-like and He-like ions are depicted in Fig. 7. These levels have been extensively studied and lifetime data are available for a very large number of ions. The early work has been reviewed by *Marrus* and *Mohr* [70].

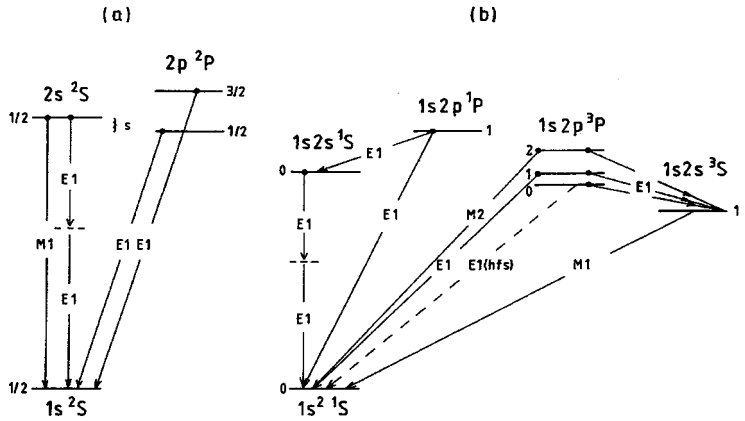

Fig. 7. Decay of n=2 levels in (a) one- and (b) two-electron ions

The $2s\ ^2S_{1/2}$ level in H-like ions decays by M1 or 2E1 emission to the ground state. These decay probabilities scale as Z^{10} and Z^6, respectively. For low values of Z, the 2E1 mode dominates while the probabilities are equal at about $Z = 41$. Experimental data, including the lifetime and branching ratio for Kr^{35}, as well as references to previous work, are given by *Cheng* et al. [53]. A 2E1 decay, similar to that for H-like ions, also takes place for the $1s2s\ ^1S_0$ level in He-like ions [71]. The photons from the 2E1 decays have a continuous frequency distribution but their sum equals the energy difference between the $n = 1$ and $n = 2$ levels.

The $1s2s\ ^3S_1$ level, already discussed above, exhibits a relativistically induced M1 decay to the $1s^2\ ^1S_0$ ground term, as first established from astrophysical observations [72]. For He-like Kr^{34+} the $^3S_1$ lifetime was determined by BFS [73]; the value, 171.0±2.0 ps, is in excellent agreement with theoretical predictions. As shown in Refs. [66, 67, 73] experimental data for this M1 transition are available for many species from He ($Z = 2$) to He-like Kr ($Z = 54$). In this interval the lifetimes range from about 8000 s (He) to 2.61 ps (Kr).

The levels $J = 0, 1, 2$ of the $1s2p\ ^3P$ term all make transitions to $1s2s\ ^3S_1$. For the $^3P_2$ level M2 transitions to the ground state are also possible. This rate scales as Z^8, and already for Ar^{16+} the M2 and E1 decay modes of $^3P_2$ are equally probable. Because of the spin–orbit interaction the wave functions of $1s2p\ ^3P_1$ and $1s2p\ ^1P_1$ are mixed, opening the spin-forbidden decay mode $1s^2\ ^1S$–$1s2p\ ^3P_1$, the transition probability of which scales as Z^{10}. Beam-foil data are here available up to He-like Ar [4].

6.3 Hyperfine Quenching

The $1s2p\ ^3P_0$ level in He-like ions has an allowed E1 decay mode to the triplet term $1s2s\ ^3S_1$. However, when the nuclear spin I differs from 0 the total angular momentum is $F = I + J$ and the $F = I$ states of the $1s2p\ ^3P_0$ and $^3P_1$ mix. Thus, transitions from $1s2p\ ^3P$ ($J = 0$, $F = 1$) to $1s^2\ ^1S$ ($J = 0$, $F = 1$) become possible. This *hyperfine quenching* which may significantly shorten the $^3P_0$ lifetime, is particularly pronounced in nuclei above $Z = 20$, as first predicted by Mohr [74]. Several additional theoretical treatments have appeared later, (see, e.g., Refs. [75, 76]), while the early experimental studies of this effect in He-like ions have been summarized by *Marrus* and *Mohr* [70].

In the early 1980s the lifetime shortening of the $1s2p\ ^3P_0$ level was demonstrated in beam-foil studies of He-like $^{19}F^{7+}$ [77], $^{27}Al^{11+}$ [78] and $^{31}P^{13+}$ [79]. The results were in excellent agreement with the theoretical data, according to which the ratio of the decay rate to the $1s^2\ ^1S_0$ ground state and to the $1s2s\ ^3S_1$ state in these three ions should be 14%, 53% and 25%, respectively [74].

In recent years experiments have been extended to heavier He-like ions, with $Z > 20$, where theories predict the hfs-induced decay branch to be much more probable than the decay to $1s2s\ ^3S_1$. As first shown by *Indelicato* et al. [75] measurements of the $1s2p\ ^3P_0$ lifetime will also allow fairly precise determinations of the $^3P_1$theoretical interest for high-Z ions where calculations are quite difficult. The first such determination, for He-like $^{107}Ag^{45+}$, was reported by *Marrus* et al. [80], resulting in a value of 0.74 eV, with an uncertainty of about 20%. This separation is, interestingly enough, smaller than the natural width of the $^3P_1$ level, 1.1 eV, the reason being that the two levels are nearly degenerate in this ion. Some years later, a more accurate beam-foil study was performed, using two isotopes, $^{107}Ag^{45+}$ and $^{109}Ag^{45+}$ [81]. The separation was now determined with a 5% uncertainty, the result being in

excellent agreement with relativistic calculations. In a similar study of He-like Ni, *Dunford* et al. [82] used both $^{61}Ni^{26+}$ ($I = 3/2$) and $^{58}Ni^{26+}$ ($I = 0$) isotopes. Here the $1s2p\ ^3P_0$ lifetime was – as expected – quite different for the two isotopes, 0.47 ns and 2.5 ns, respectively, whereas the fine structure was determined with an uncertainty of 6%. Subsequently, a similar measurement was extended to the isotopes $^{155}Gd^{62+}$ and $^{157}Gd^{62+}$ [83]. While both nuclei have $I = \frac{3}{2}$, the nuclear magnetic moments are different, resulting in different $1s2p\ ^3P_0$ lifetimes. A very accurate value was now obtained for the fine structure splitting, the uncertainty being only 1%.

7. Conclusion

The examples of lifetime measurements for highly charged ions and the interplay of the experimental results with data from theoretical and semiempirical analyses discussed in this review should demonstrate that the field of lifetime studies for highly ionized atoms is still in a very active phase. The method of BFS which has been used for more than 30 years now produces data which are more reliable than ever before. At the same time new techniques (storage rings, ion traps) for determination of long lifetimes are yielding data with uncertainties below 1%, thereby providing accurate tests of advanced theoretical methods. This precision is thus comparable to that reached in laser-based lifetime experiments of neutral atoms such as Li, Na and Cs [84].

In view of the developments on the theoretical side, it now appears desirable to further develop experimental techniques in such a way that typical uncertainties in experimental data reach the 1–3% level, instead of 5–10% which appears to be common in most lifetime studies for highly ionized atoms. In this way it would be possible to obtain information about various subtle effects in such ions. While the cascading problems are largely understood and solved in the BFS case, there are additional difficulties when the ion energies are tens of MeV or even higher. Among these are line blends and high beam-dependent backgrounds. Thus, lifetime measurements must be preceded by or combined with detailed spectroscopic studies of the systems of interest whereas the background problems caused by electrons or x rays require careful designs of the experimental setup. Another practical limitation is caused by the fact that the available time for experiments at large ion accelerators is usually quite limited. However, here the introduction of position-sensitive detectors, in particular charge-coupled detectors (CCD), have increased the data-recording efficiency by orders of magnitude.

Acknowledgement. The authors are grateful to the US Department of Energy, Office of Basic Energy Sciences, Division of Chemical Sciences and to the Swedish Natural Sciences Research Council (NFR) for support during the preparation of this work.

References

1. R.K. Janev: Comm. At. Mol. Phys. **26**, 83 (1991)
2. D.S. Leckrone, S. Johansson, G.M. Wahlgren, S.J. Adelman: Phys. Scr. **T47**, 149 (1993)
3. U. Feldman, W.E. Behring, W. Curdt, U.Schüle, K. Wilhelm, P. Lemaire, T.M. Moran: Astrophys. J. Suppl. Ser. **113**, 195 (1997)
4. I. Martinson: Lithuanian J. Phys. **36**, 3 (1996)
5. L.J. Curtis: in *Atomic Molecular and Optical Physics Reference Book*, G.W.F. Drake ed. (AIP Press, New York 1996) pp. 206–212
6. E. Träbert: in *Accelerator-Based Atomic Physics: Techniques and Applications*, S.M. Shafroth and J.C. Austin, eds. (AIP Press, New York 1998) pp. 567–600
7. L.J. Curtis, I. Martinson: Comm. At. Mol. Phys. **24**, 213 (1990)
8. E.H. Pinnington: in *Atomic Molecular and Optical Physics Reference Book*, G.W.F. Drake ed. (AIP Press, New York 1996) pp. 213–219
9. R.K. Janev, L.P. Presnyakov, V.P. Shevelko: *Physics of Highly Charged Ions*, (Springer-Verlag, Berlin 1985)
10. T.R. O'Brian, J.E. Lawler: in *Atomic, Molecular and Optical Physics: Atoms and Molecules*, F.B. Dunning and R.G. Hulet, eds. (Experimental Methods in the Physical Sciences, R. Celotta and T. Lucatorto, eds., Vol. 29B, Academic Press, San Diego 1996) pp. 217–254
11. H.-P. Garnir, T. Bastin, P.-D. Dumont: Phys. Scr. **T65**, 36 (1996)
12. E. Träbert: Nucl. Instrum. Methods B **98**, 10 (1995)
13. L. Engström: Phys. Scr. **40**, 17 (1989)
14. L.J. Curtis, P. Erman: J. Opt. Soc. Am. **67**, 1218 (1977)
15. L.J. Curtis: J. Opt. Soc. Am. **64**, 495 (1974)
16. G. Hubricht, E. Träbert: Z. Phys. D **7**, 243 (1987)
17. L.J. Curtis: in *Beam Foil Spectroscopy*, S. Bashkin ed. (Berlin, Springer 1976) pp. 63–109
18. S.W. Provencher: J. Chem. Phys. **64**, 2772 (1976)
19. L.J. Curtis, H.G. Berry, J. Bromander: Phys. Lett. **34** A, 169 (1971)
20. M. Henderson, L.J. Curtis, R. Matulioniene, D.G. Ellis, C.E. Theodosiou: Phys. Rev. A **56**, 1872 (1997)
21. L. Engström: Nucl. Instrum. Methods **202**, 369 (1982)
22. L. Engström, P. Bengtsson, C. Jupén, A.E. Livingston, I. Martinson: Phys. Rev. A **51**, 179 (1995)
23. A.E. Livingston, F.G. Serpa, A.S. Zacarias, L.J. Curtis, H.G. Berry, S.A. Blundell: Phys. Rev. A **44**, 7820 (1991)
24. E. Träbert, J. Sulieman, S. Cheng, H.G. Berry, R.W. Dunford, E.W. Kanter, C. Kurtz, A.E. Livingston, K.W. Kukla, F.G. Serpa, L.J. Curtis: Phys. Rev. A **47**, 3805 (1993)
25. R.D. Cowan: *The Theory of Atomic Structure and Spectra*, (Univ. California Press, Berkeley 1981)
26. L.J. Curtis, R.T. Deck, D.G. Ellis: Phys. Lett. A **230**, 330 (1997)
27. I. Lindgren: Nucl. Instr. Meth. Phys. Res. B **31**, 102 (1988)
28. C.E. Theodosiou, L.J. Curtis: Phys. Rev. A **38**, 4435 (1988)
29. U.I. Safronova, V.S. Senashenko: Phys. Scr. **25**, 37 (1982)
30. C. Froese-Fischer: Comput. Phys. Commun. **64**, 369 (1991)
31. A. Hibbert: Comput. Phys. Commun. **9**, 151 (1975)
32. C. Froese-Fischer, M. Godefroid, J. Olsen: J. Phys. B **30**, 1163 (1997)
33. J. Fleming, A. Hibbert, R.P. Stafford: Phys. Scr. **49**, 316 (1994)

34. H.A. Bethe, E.E. Salpeter: *Quantum Mechanics of One- and Two-Electron Atoms* (Springer, Berlin 1957)
35. F. Parpia, C. Froese-Fischer, I.P. Grant: Comput. Phys. Commun. **94**, 249 (1996)
36. W.R. Johnson, K.-N. Huang: Phys. Rev. Lett. **48**, 315 (1982)
37. H.-S. Chou, H.-S. Chi, K.-N. Huang: Chin. J. Phys. B **32**, 261 (1994)
38. A.-M. Mårtensson-Pendrill: Phys. Scr. **T46**, 102 (1993)
39. J. Sapirstein: Phys. Scr. **T46**, 52 (1993)
40. M.W. Smith, W.L. Wiese: Astrophys. J. Suppl. Ser. **23**, 103 (1971)
41. M. Cohen, A. Dalgarno: Proc. Roy. Soc. A **280**, 258 (1964)
42. R.J.S. Crossley, A. Dalgarno: Proc. Roy. Soc. A **286**, 510 (1965)
43. B. Edlén: Phys. Scr. **17**, 565 (1978)
44. L.J. Curtis, D.G. Ellis, I. Martinson: Phys. Rev. A **51**, 251 (1995)
45. J. Schweppe, A. Belkacem, L. Blumenfeld, N. Claytor, B. Feinberg, H. Gould, V.E. Kostroun, L. Levy, S. Misawa, J.R. Mowat, M.H. Prior: Phys. Rev. Lett. **66**, 1434 (1991)
46. L.J. Curtis: Phys. Scri. **43**, 137 (1991)
47. E. Träbert, L.J. Curtis: Phys. Scr. **48**, 586 (1993)
48. L.J. Curtis: J. Phys. B **26**, L589 (1993)
49. M. Henderson, L.J. Curtis: J. Phys. B **29**, L629 (1996)
50. L.J. Curtis, D.G. Ellis: J. Phys. B **29**, 645 (1996)
51. L.J. Curtis, D.G. Ellis, R. Matulioniene, T. Brage: Phys. Scr. **56**, 240 (1997)
52. L.J. Curtis, S.T. Maniak, R.W. Ghrist, R.E. Irving, D.G. Ellis, M. Henderson, M.H. Kacher, E. Träbert, J. Granzow, P. Bengtsson, L. Engström: Phys. Rev. A **51**, 4575 (1995)
53. S. Cheng, H.G. Berry, R.W. Dunford, D.S. Gemmell, E.P. Kanter, B.J. Zabransky, A.E. Livingston, L.J. Curtis, J. Bailey, J.A. Nolen, Jr.: Phys. Rev. A **47**, 903 (1993)
54. M. Henderson, L.J. Curtis, D.G. Ellis, R.E. Irving, G.M. Wahlgren: Astrophys. J. **473**, 565 (1996)
55. A.E. Livingston, H.G. Berry: Phys. Rev. A **17**, 1966 (1977)
56. L. Engström: Phys. Scr. **28**, 68 (1983)
57. E. Träbert: Phys. Scr. **48**, 699 (1993)
58. D. Schneider: this volume
59. B.J. Wargelin, P. Beiersdorfer, S.M. Kahn: Phys. Rev. Lett. **71**, 2196 (1993)
60. G.S. Stefanelli, P. Beiersdorfer, V. Decaux, K. Widmann: Phys. Rev. A **52**, 3651 (1995)
61. F.G. Serpa, C.A. Morgan, E.S. Meyer, J.D. Gillaspy, E. Träbert, D.A. Church, E. Takács: Phys. Rev. A **55**, 4196 (1997)
62. M. Larsson: Rep. Prog. Phys. **58**, 1267 (1995)
63. P.H. Mokler, Th. Stöhlkler: Adv. At. Mol. Opt. Phys. **37**, 297 (1996)
64. A. Wolf: this volume
65. I. Klaft, S. Borneis, T. Engel, B. Fricke, R. Greiser, G. Huber, T. Kühl, D. Marx, R. Neumann, S. Schröder, P. Seelig, L. Völker: Phys. Rev. Lett. **73**, 2425 (1994)
66. H.T. Schmidt, P. Forck, M. Grieser, D. Habs, J. Kenntner, G. Miersch, R. Reprow, U. Schramm, T. Schüssler, D. Schwalm, A. Wolf: Phys. Rev Lett. **72**, 1616 (1994)
67. H. Schmidt: Ph.D. thesis, Aarhus University (1994)
68. J. Doerfert, E. Träbert, A. Wolf, D. Schwalm, O. Uwira: Phys. Rev. Lett. **78**, 4355 (1997)
69. J. Doerfert, E. Träbert: Nucl. Instrum. Methods B **99,** 124 (1995)
70. R. Marrus, P.J. Mohr: Adv. Atom. Molec. Phys **14**, 181 (1978)

71. R.W. Dunford, H.G. Berry, S. Cheng, E.P. Kanter, C. Kurtz, B.J. Zabransky, A.E. Livingston, L.J. Curtis: Phys. Rev. A **48**, 1929 (1993)
72. A.H. Gabriel, C. Jordan: Phys. Lett **32** A, 166 (1970)
73. S. Cheng, R.W. Dunford, C.J. Liu, B.J. Zabransky, A.E. Livingston, L.J. Curtis: Phys. Rev. A **49**, 2347 (1994)
74. P.J. Mohr: in *Beam-Foil Spectroscopy*, I.A. Sellin and D.J. Pegg, eds. (Plenum Press, New York 1976) p. 97
75. P. Indelicato, F. Parente, R. Marrus: Phys. Rev. A **40**, 3505 (1989)
76. A. Aboussaid, M.R. Godefroid, P. Jönsson, C. Froese-Fischer: Phys. Rev. A **51**, 2031 (1995)
77. L. Engström, C. Jupén, B. Denne, S. Huldt, Weng Tai Meng, P. Kaijser, U. Litzén, I. Martinson: J. Phys. B **13**, L143 (1980)
78. B. Denne, S. Huldt, J. Pihl, R. Hallin: Phys. Scr. **22**, 45 (1980)
79. A.E. Livingston, S. Hinterlong: Nucl. Instrum. Methods **202**, 103 (1982)
80. R. Marrus, A. Simionovici, P. Indelicato, D.D. Dietrich, P. Charles, J.-P. Briand, K. Finlayson, F. Bosch, D. Liesen, F. Parente: Phys. Rev. Lett. **63**, 502 (1989)
81. B.B. Birkett, J.-P. Briand, P. Charles, D.D. Dietrich, K. Finlayson, P. Indelicato, D. Liesen, R. Marrus, A. Simionovici: Phys. Rev. A **47**, R2454 (1993)
82. R.W. Dunford, C.J. Liu, J. Last, N. Berrah-Mansour, R. Vondrasek, D.A. Church, L.J. Curtis: Phys. Rev. A **44**, 764 (1991)
83. P. Indelicato, B.B. Birkett, J.-P. Briand, P. Charles, D.D. Dietrich, R. Marrus, A. Simionovici: Phys. Rev. Lett. **68**, 1307 (1992)
84. C.E. Tanner: in *Atomic Physics 14*, D.J. Wineland, C.E. Wieman and S.J. Smith, eds (AIP, New York 1995) pp. 130–145